The International Journal of Advanced Manufacturing Technology (2023) 125:1229–1238
https://doi.org/10.1007/s00170-023-10803-9

ORIGINAL ARTICLE

Deformation length in flexible roll forming

Hassan Badparva[1] · Hassan Moslemi Naeini[1] · Mohammad Mehdi Kasaei[2,3] · Yaghoub Dadgar Asl[4] · Behnam Abbaszadeh[1] · Lucas F. M. da Silva[5]

Received: 12 September 2022 / Accepted: 31 December 2022 / Published online: 6 January 2023

Abstract
Flexible roll forming (FRF) is a novel sheet metal process for innovative manufacturing of variable cross-section profiles which are especially needed in the automotive industry to construct lightweight structures. One of the important parameters of the flexible roll forming process is deformation length which plays a key role in the design of interstand distance. This paper presents a new understanding on the deformation length in the flexible roll forming process by performing experimental tests and numerical simulations. Results show that in flexible roll forming, unlike conventional roll forming, the deformation length varies considerably in such a way that the maximum and minimum values of the deformation length appear in the stretching and compression zones, respectively. Hence, it is recommended that the deformation length in the stretching zone is considered for designing the interdistance of stands. Results also allow concluding that the increase of the forming angle α, flange length F, and yield strength Y and the decrease of thickness t increase the deformation length in all the regions of a variable cross-section profile.

Keywords Flexible roll forming · Variable cross-section profile · Deformation length · Longitudinal strain · Automotive industry

1 Introduction

Roll forming has been extensively used to produce a wide range of profiles in the automotive industry, construction sector, and oil and gas industry due to the advantages, including high-speed and continuous production, high-quality products, and energy savings. In this process, a desired profile is progressively formed by passing a long metal strip through a set of rotating rolls [1]. One of the limitations of the conventional roll forming process is the inability to produce variable cross-section profiles. To overcome this limitation, flexible roll forming (FRF) has been developed [2]. In this process, the rolls are not fixed at their position, and translate and rotate to form the bending line of a desired profile (see Fig. 1). These translational and rotational movements of the rolls are calculated according to the geometry of the profile and controlled by a computer numerical control system (CNC). FRF has received much attention in the automotive industry for producing complex and load optimized profiles with variable cross-section, which are especially required to reduce the weight of body-in-whites [3, 4].

One of the important parameters of the FRF process is the length of the region where deformation occurs between successive stands. This parameter, called "deformation length," plays an essential role in determining the distance between stands [5]. Figure 2 shows the deformation length in the stretching zone of a variable cross-section channel profile. Since the deformation starts at the sheet edge, its longitudinal strain is usually examined to determine the deformation length.

Bhattacharyya et al. [6] proposed an equation for predicting the deformation length in the conventional roll forming

✉ Mohammad Mehdi Kasaei
mkasaei@inegi.up.pt

1 Faculty of Mechanical Engineering, Tarbiat Modares University, Tehran, Iran

2 Institute of Science and Innovation in Mechanical and Industrial Engineering, Porto, Portugal

3 Department of Mechanical Engineering, Qazvin Branch, Islamic Azad University, Qazvin, Iran

4 Department of Mechanical Engineering, Tehran Branch, Faculty of Enghelab-E Eslami, Technical and Vocational University, Tehran, Iran

5 Department of Mechanical Engineering, Faculty of Engineering, University of Porto, Porto, Portugal

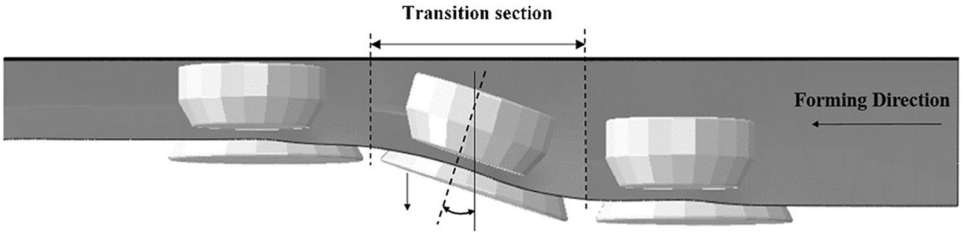

Fig. 1 Schematic representation of the roll movements in the FRF process

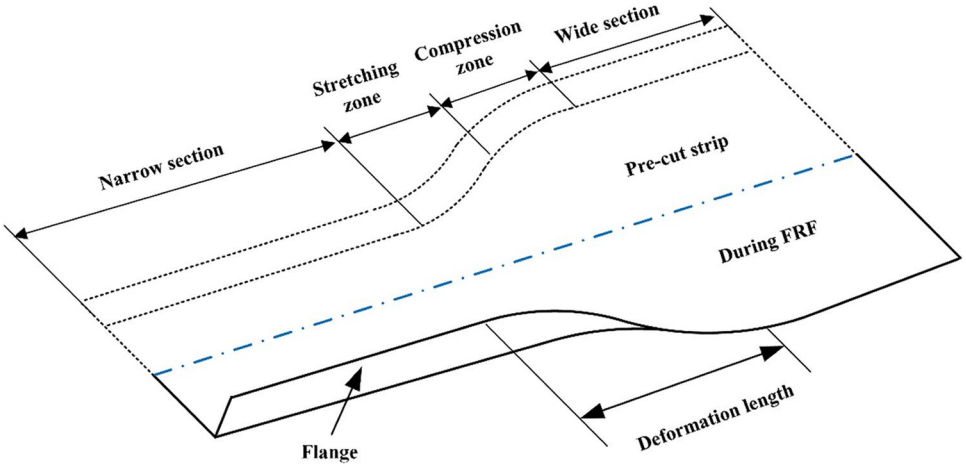

Fig. 2 Schematic representation of the deformation length in the stretching zone during the FRF of a variable cross-section channel profile

process by minimizing the deformation energy and assuming a rigid-perfectly plastic model for the material. This equation is a function of sheet thickness, flange length, and forming angle. Azizi Tafti et al. [7] modified the model proposed by Bhattacharyya et al. [4] by considering the elastic-perfectly plastic behavior. Liu et al. [8] proposed a new mathematical model for obtaining the distribution of bending angle and edge longitudinal strain in the roll forming process. The influence of flange length and roll diameter on the peak longitudinal strain was also investigated. Safdarian and Moslemi [8] investigated the effects of the roll forming parameters of a channel profile on the edge longitudinal strain. It was showed that the increase of the interstand distance decreases the peak and residual longitudinal strains and concluded that forming condition can be better when the interstand distance increases. However, a higher interstand distance increases roll forming machine cost and process time and intensifies the springback of the deformed sheet.

Abeyrathna et al. [9] developed a geometric model in which longitudinal edge strain can be calculated as function of the forming angle, the flange length, and the interdistance of stands. In fact, the effects of material behavior, thickness, and roll diameter were ignored in this model. Sun et al. [10] established a simplified analytical model, solely based on the geometric parameters to estimate the longitudinal strain in chain-die forming, a recently proposed manufacturing method similar to roll forming, a channel profile. Qiana et al. [11] proposed a semianalytical model using the numerical simulation of a multistand chain-die forming process to predict the minimum interdistance of the forming stands.

To authors' knowledge, in the FRF process, the deformation length has not been studied so far, and most of the researches have been focused on understanding the deformation mechanics in FRF and recognizing the causes of the forming defects such as wrinkling, warping, and longitudinal bow. Kasaei et al. [12] showed that the deformation in the transition section of a variable cross-section profile is a combination of flanging and conventional roll forming processes. Kasaei et al. [2] analyzed the deformation mechanics of FRF using the combined evolution of in-plane stresses and strains with time. They [13] developed a formability test to characterize the wrinkling limit curve (WLC) and proposed the analysis of loading path's evolutions against the WLC in the space of effective strain versus stress triaxiality to understand and predict the occurrence of flange wrinkling.

Rezaei et al. [14] showed that as the strain created at the flange edge gets closer to the desired strain, the web warping defect decreases. Accordingly, a cost-effective method based on the design of the bend curve was proposed to reduce this defect. Woo et al. [15] reported the transversal nonuniformity of the longitudinal strain as the main cause of longitudinal bow in flexible roll-formed profiles.

Dadgar Asl et al. [16] investigated the influence of the sheet thickness, forming angle, and bending radius on ductile fracture in FRF. Dadgar Asl et al. [17] performed a nonsorting multiobjective optimization to minimize the

flange wrinkling and the longitudinal bow using artificial neural networks. Kasaei et al. [18] proposed a new criterion based on the WLC in the space of effective strain versus stress triaxiality to predict the risk of wrinkling in finite element analysis. This criterion was employed to determine the critical forming angle in FRF, and the flange length, yield strength, and sheet thickness were reported as the most important parameters affecting the occurrence of wrinkling. Abeyrathna et al. [19] investigated the FRF of an automotive part made from advance high strength steels and tried to reduce the defects such as end flare, spring back, and wrinkling by applying a overbending approach and controlling forming sequence. The distance between the stands can affect the deformation of the sheet and, as a result, forming defects. A necessary condition to correctly determine this vital parameter is to know the deformation length.

Unlike the conventional roll forming process, the deformation length is expected to change during FRF, due to the changes in the cross-section of the profile. Thus, the existing knowledge about the deformation length needs to be revisited for the FRF process. In this paper, the deformation length in FRF is investigated using experimental and numerical simulations. The relationship between the deformations applied to flange edge and the deformation length are analyzed. In addition, the effects of geometric parameters of the variable cross-section channel profile and material properties of the sheet on the deformation length are determined.

2 Experimentation

2.1 Material characterization

The experimental tests were conducted on St12 steel sheets with 0.5 mm thickness. The mechanical properties of the material were obtained from uniaxial tensile tests in three directions of 0°, 45°, and 90° with respect to the rolling direction. The tests were performed according to ASTM E8 by means of a universal test machine Instron 4507. The mechanical properties and anisotropic characteristics of the material are given in Tables 1 and 2, respectively. The stress–strain curve was modeled by Ludwik-Hollomon law as follows:

$$\sigma = 586.8\varepsilon^{0.286}\text{MPa} \tag{1}$$

The onset of plastic deformation was defined by the Hill 1948 anisotropic yield criterion, which is represented as follows:

$$f(\sigma) = \sqrt{F\left(\sigma_{yy}-\sigma_{zz}\right)^2 + G\left(\sigma_{zz}-\sigma_{xx}\right)^2 + H\left(\sigma_{xx}-\sigma_{yy}\right)^2 + 2L\sigma_{yz}^2 + 2M\sigma_{zx}^2 + 2N\sigma_{xy}^2} \tag{2}$$

where σ_{ij} is stress components and F, G, H, L, M, and N are the constants that describe the material anisotropy. The contents can be calculated based on the Lankford coefficients r_0, r_{45}, and r_{90} with the assumption of the associated flow rule in the plane stress state as follows:

$$\begin{aligned} F &= \frac{r_0}{r_{90}\left(r_0+1\right)}; G = \frac{1}{r_0+1}; \\ H &= 1-G; L = M = 1.5; \\ N &= \frac{\left(r_0+r_{90}\right)\bullet\left(1+2r_{45}\right)}{2r_{90}\left(r_0+1\right)} \end{aligned} \tag{3}$$

The Hill 1948 yield criterion constants of the St12 steel sheets with 0.5 mm thickness are given in Table 2.

2.2 Experiments in flexible roll forming

Experiments were performed by a single forming stand FRF setup shown in Fig. 3. In this setup, the translational and rotational movements of the rolls are provided by a parallel kinematic mechanism with two axes. A specialized feeding mechanism pulls the sheet through the rolls with an adjustable velocity. The mechanisms of the FRF setup are controlled by a PC-based control unit that was developed upon on a personal computer equipped with a LabVIEW-based software and a data acquisition board. A supporting stand was employed to guide the sheet to enter into the forming stand. More information about the FRF setup is available elsewhere [2].

In this study, the target profile is a symmetric channel profile with variable width (Fig. 4). The width of the wide section W_2 is twice the width of the narrow section W_1. These two sections are connected to each other through a transition section that consists of two curved flanges with tangent circular bend curves. Although the lengths of the bend curves (with radius of R) are similar, lengths of the edge curves are not equal in

Table 1 Mechanical properties of the St12 steel sheets with 0.5 mm thickness

Modulus of elasticity, E (G Pa)	Yield strength, Y (MPa)	Ultimate tensile strength, UTS (MPa)	Elongation at break, A (%)
196.53	173.27	327.68	55.26

Table 2 Anisotropic characteristics and the Hill's 48 criterion constants of the St12 steel sheets with 0.5 mm thickness

Lankford coefficient			Normal anisotropy,$\bar{r}$	Planar anisotropy,Δr	Hill's 48 criterion					
r_0	r_{45}°	r_{90}			F	G	H	L	M	N
1.32	1.23	1.55	1.3	0.2	0.46	0.39	0.61	1.5	1.5	1.48

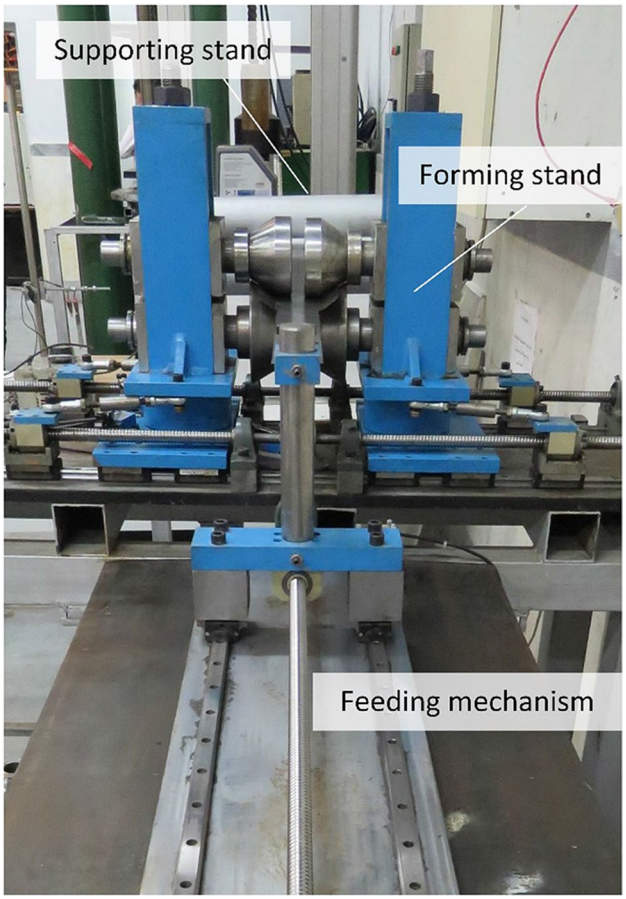

Fig. 3 Flexible roll forming setup

these concave and convex parts. To produce a sound profile, the shorter curve with radius of R_1 should be stretched and the longer one with radius of R_2 should be compressed during the deformation. For this reason, these concave and convex parts are called the stretching and compression zones, respectively. The geometric parameters of the profile and a half of its precut strip are shown in Fig. 4. The values of geometric parameters are given in Table 3. The precut strips were cut by a laser cutting machine from the supplied sheets in such a way that their longitudinal direction coincided with the sheets' rolling direction.

Table 3 Values of the geometric parameters in the FRF experiments

Parameter	Value
W_1(mm)	70
W_T(mm)	35
R(mm)	400
F(mm)	30
α(deg)	30
t(mm)	0.5

To measure the deformation length in the different regions of the profile, the process was stopped in the middle of each region. Then, the semiformed profile was removed from the forming stand by increasing the gap between the top and bottom rolls. The semiformed profiles are shown in Fig. 5.

The semiformed profiles were placed on the table, and the photos were taken from their side view (see Fig. 6). Then, the coordinates of several points on the flange edge were obtained by Plot Digitizer software. It was assumed that the deformation begins at a point on the edge where was 0.5 mm above the plane of the undeformed sheet. Finally, the horizontal distance between this point and the last point that was in contact with the midsection of the forming rolls was measured as the deformation length (Fig. 6).

To evaluate the effect of springback on the obtained values, the deformation length was also measured in the narrow and wide sections before removing the semiformed profiles from the stand. The results showed that the difference in the measured deformation lengths is less than 4%, which can be related to the concentration of the deformation in the flange and bend areas and the low strength of the material leading to a low springback tendency.

3 Finite element modeling

The ABAQUS software with a quasistatic implicit formulation was employed to simulate the FRF process. The rolls were assumed to be rigid due to their negligible

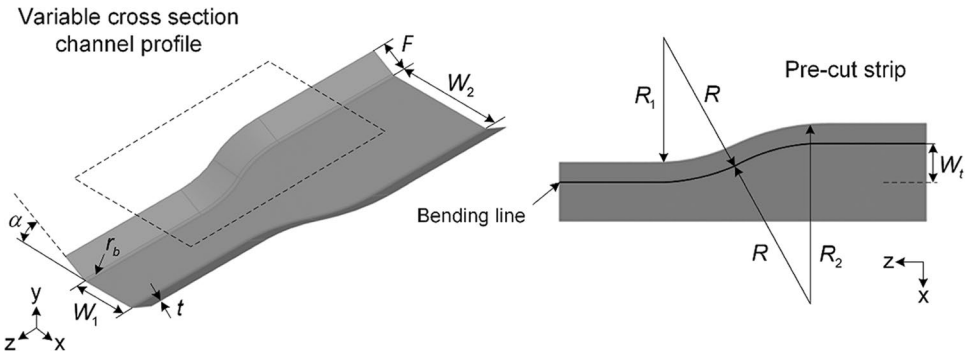

Fig. 4 Geometric parameters of the target profile and its pre-cut strip

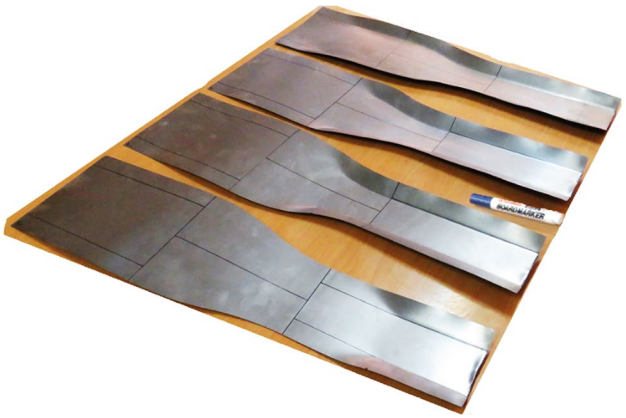

Fig. 5 The semiformed profiles for measuring the deformation length in the different regions of the variable cross-section profile

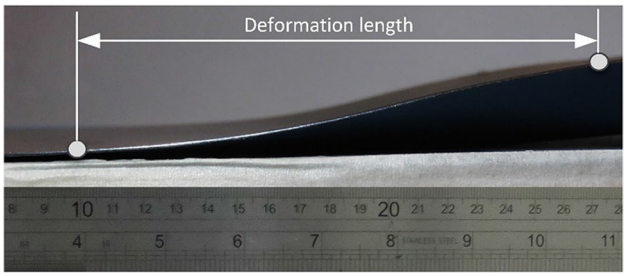

Fig. 6 Photograph showing the side view of the semi formed profile for measuring the deformation length

elastic deformation, while the sheet was modeled as a deformable part with elastic–plastic behavior. The sheet was discretized by S4R quadratic shell elements.

Due to the symmetry of the studied profiles, only half of the sheet and the rolls were modeled. The first stand was used to guide the sheet during FRF. The trapezoidal rolls of the second stand were responsible for the deformation. By defining required boundary conditions, the forming rolls were moved linearly along the X-axis and rotated around the Y-axis to form the bending line of the profile in the transition section. A displacement boundary condition was also defined at the front edge in order to pull the sheet through the gaps of the rolls similar to the experiments.

The Hill's 48 plasticity criterion were applied to model the anisotropic behavior of the material and isotropic strain hardening was considered. The material flow stress was predicted by defining the points of the true stress-plastic strain curve in the software. To this end, the true stress–strain curve obtained from Eq. 1 was converted to the true stress-plastic strain curve. A penalty-based method with a Coulomb friction law was utilized to replicate the contact with friction between the sheet and the rolls. The friction coefficient of 0.1 was considered. Figure 7 shows the assembly of the discretized sheet and the rolls and the distribution of von Mises stress in the end of the simulation.

The finite element simulations were used to investigate the effects of the profile geometry and material properties on the deformation length in FRF. The variables are the flange length F, forming angle α, and sheet thickness t, which were reported as the effective parameters on the deformation length in the conventional roll forming [6], along with yield strength Y. For each variable, three values were considered according to Tables 4. When examining each variable, the other variables were assumed in the central values. The stress–strain curves were modeled using the Ludwik-Hollomon equation so that the hardening exponent n was constant while the strength coefficient K was proportional to the yield strength Y.

The deformation length was obtained from the finite element analysis by doing the following steps:

1. A path was defined on the flange edge before the forming stand as shown in Fig. 8.
2. The longitudinal strain in the middle layer was obtained on the defined path.
3. The horizontal distance between the beginning of the deformation and the node in contact with the midsection of the forming rolls was measured as the deformation length.

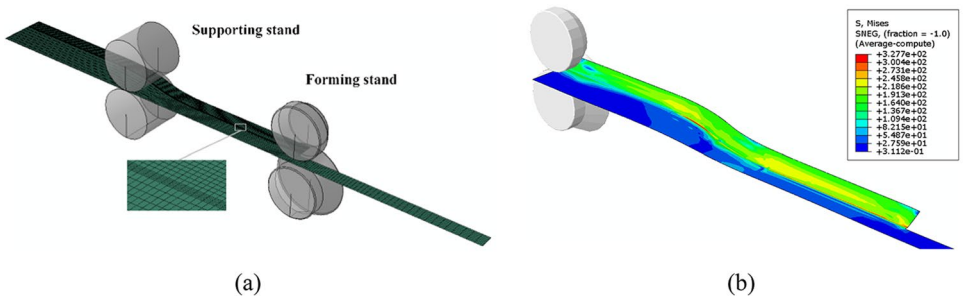

Fig. 7 The finite element model of the FRF process according to the experiments (**a**) and the contour plot of von Mises stress after the forming process (**b**)

Table 4 Values of the parameters in the FRF simulations

Category	Parameter	Value		
Profile geometry	W_1(mm)	70		
	W_T(mm)	35		
	R(mm)	400		
	F(mm)	10	20	30
	α(deg)	10	20	30
Material properties	t(mm)	0.5	1	1.5
	Y(MPa)	150	400	650
	n	0.2		
	K(MPa)	$E^n Y^{1-n}$		

4 Results and discussion

4.1 Validation of the finite element model

In order to validate the finite element model, a comparison was made between the deformation lengths obtained from the finite element simulation and the experiments for the variable cross-section profile with the geometric parameters given in Table 3. As seen in Table 5, the relative difference between the finite element-predicted and experimental results in the different regions is less than 9% that reveals a good agreement. The springback of the deformed sheets in the experiments, as previously mentioned, can be a reason for the difference between experimental and simulation results. It should be noted that the validity of this model was previously confirmed by comparing the numerical and experimental results for the history of the longitudinal strain and web centerline shape [18].

Further analysis of Table 5 shows that the deformation length in the FRF process, unlike the conventional roll forming process, is not constant. The maximum and minimum deformation lengths were obtained in the stretching and compression zones, respectively, that shows a relative change of 16%. However, the deformation lengths of the narrow and wide sections are similar. The causes of these changes should be sought in the deformation modes of flange in the four regions of the variable cross-section profile, which will be discussed in the following section.

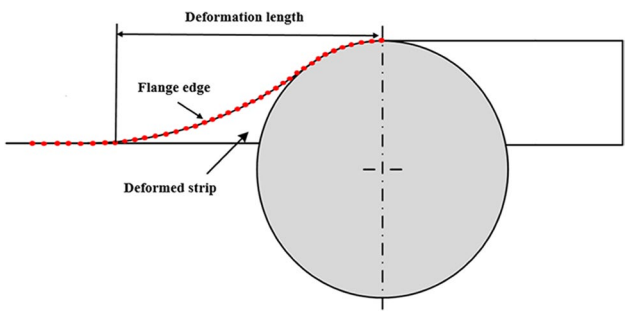

Fig. 8 Method utilized for obtaining the deformation length from the finite element simulation

Table 5 Comparison of the deformation lengths obtained from the finite element simulation and experiments

Region	Deformation length (mm)		Relative difference (%)
	FEM	Experiment (mm)	
Narrow section	157.38	172.35	8.6%
Stretching zone	182.37	193.5	5.6%
Compression zone	154.3	166.8	7.2%
Wide section	156.5	169.2	7.5%

4.2 Deformation length in FRF

To understand the deformation length in FRF, the deformations of the flange edge at the different sections should be examined. Figure 9 shows the history of the longitudinal strain for the central levels of Tables 4. The selected material points are located on the flange edge at the middle of each region.

The deformations can be considered at two regions (see Fig. 10). The first region is from the beginning of the deformation until the midsection of the forming rolls. The second region initiates immediately after the first region and continues until the flange is completely deformed. From the beginning of the first region to the moment that the flange edge enters in contact with the bottom roll, the material experiences a combination of longitudinal bending (D1) and uniaxial tension (D2), because of the movement of the flange edge along a spatial path. The length

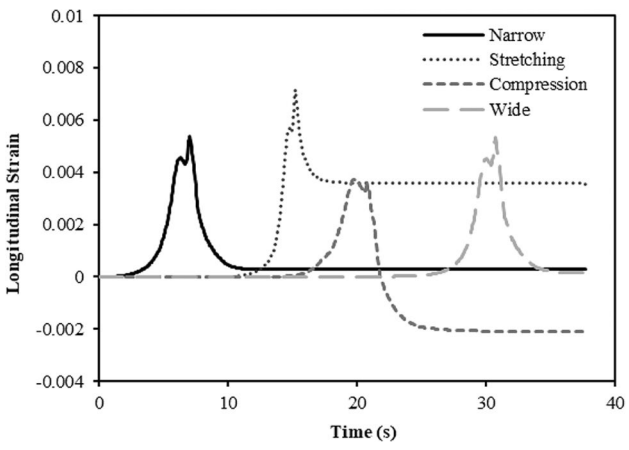

Fig. 9 Evolution of the longitudinal strain with time at the flange edge in the four regions of the variable cross-section for central values of Tables 5

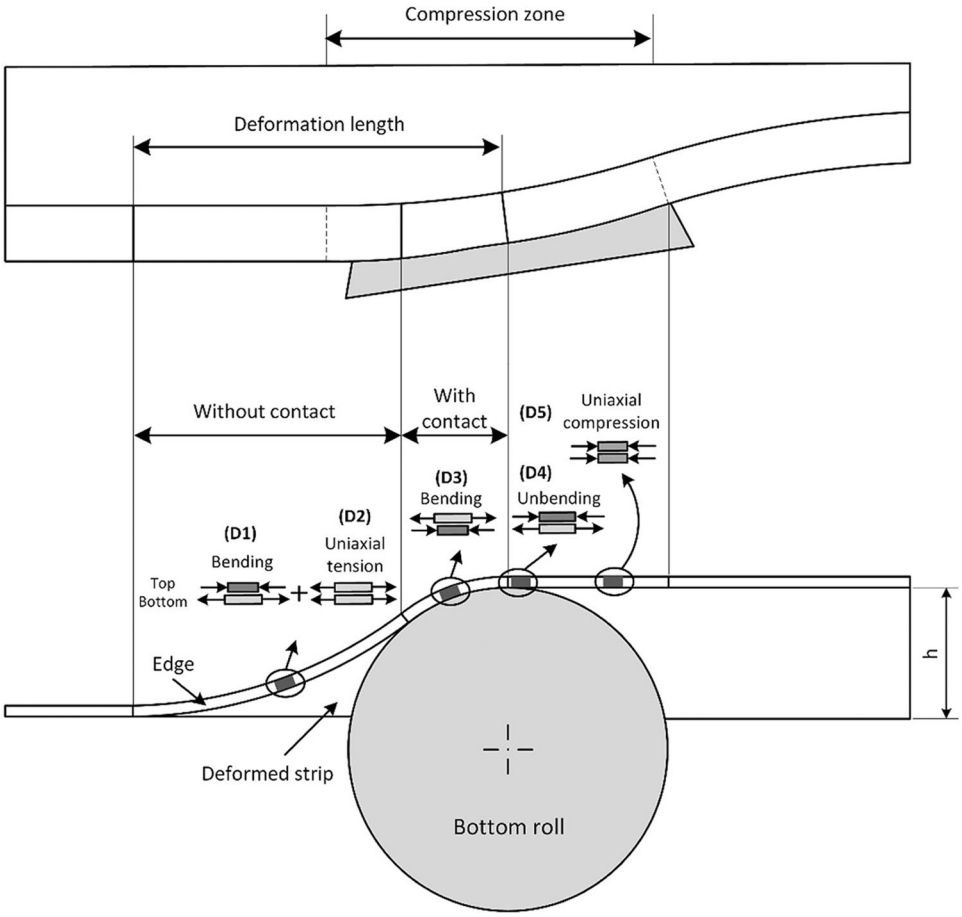

Fig. 10 Schematic representation of the deformations of the flange edge and its relationship with the deformation length in FRF

of this spatial path is greater than the initial length of the edge of the sheet therefore the flange edge is stretched by moving it along the path. A longer spatial path results a more tension at the flange edge.

When the flange edge comes in contact with the rolls, it is longitudinally bent (D3) by the bottom roll. The strain at this area is dependent on the radius of the bottom roll at the contact point with the flange edge. The peak longitudinal strain usually appears in the middle of the contact area, which is the result of strains in the contact and non-contact areas. As seen in Fig. 9, the maximum and minimum values of the peak longitudinal strain occur in the stretching and compression zones, respectively, while in the narrow and wide sections, the peak values are the same. These differences in the peak values are due to differences in flange geometry that affect the deformations of the flange edge. In the stretching region, the length of the flange edge is initially smaller than the length of the bend curve, while in the compression zone it is the opposite. Therefore, a more tension is applied to the flange and the highest peak is formed during the deformation of the stretching zone. Since the initial lengths of the flange edge and the bend line are equal in the narrow and wide sections, the values of the peak longitudinal strain in these two sections are equal and located between the peak values of the stretching and compression zones.

Because of the local bending deformation (D3), an unbending (D4) happens at the edge after passing the flange through the rolls. As the flange moves further, a uniaxial compression (D5) is applied to the flange in order to reduce the longitudinal strain to a level very close to the residual strain required to attain the desired flange with flat, concave or convex shapes [18]. Among the abovementioned deformations, the ones that belong to the first region affect the deformation length (D1, D2, and D3). Thus, the deformation length can be expected to increase by increasing these deformations. The deformation lengths were obtained 98, 112, 86, and 98 mm for the narrow section, stretching and compression zones, and wide section, respectively, which the observed trend is well matched to that of the peak longitudinal strains. Consequently, it can be concluded that in a given profile, the higher the peak longitudinal strain, the larger the deformation length is formed.

4.3 Effect of forming angle α

Figure 11 shows the influence of the forming angle α on the deformation length in the different regions of the variable

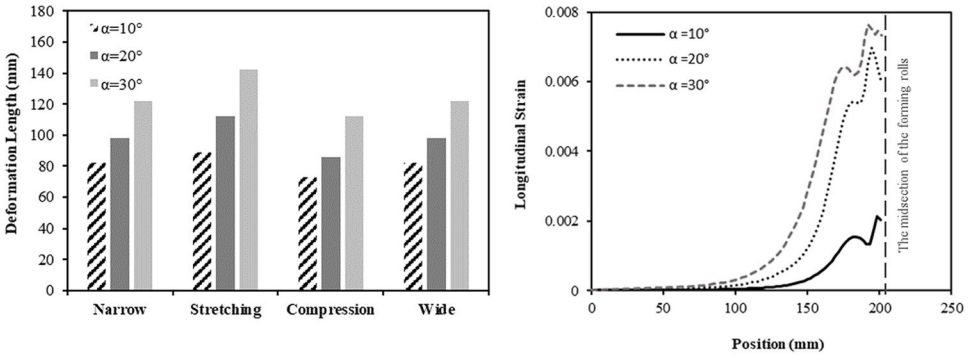

Fig. 11 Effects of forming angle α on the deformation length (**a**) and the longitudinal strain along the path at the flange edge when forming the stretching zone (**b**)

cross-section profile and the longitudinal strain during the deformation of the stretching zone. The stretching zone was chosen because it has the longest deformation length. As seen in Fig. 11a, the deformation length increases in all four regions of the variable cross-section profile by increasing the forming angle from 20° to 40°. The increases of the deformation length in the narrow and wide sections are the same and equal to 48%, while those in the stretching and compression zones are 59% and 54% respectively. With a higher forming angle, the height h of the flange edge in contact with the bottom roll increases. As a result of this, the length of the spatial path of the flange edge increases and a more tension is applied to the flange edge. As shown in Fig. 11b, the longitudinal strain at the flange edge of the profile rises sooner and higher as the forming angle increases that justifies the cause for the increase in deformation length.

4.4 Effect of flange length *F*

The changes of the deformation length with the flange length F are shown in Fig. 12a. As the flange length increases from 10 to 30 mm, the deformation length in the constant cross-section regions increases by 76%, while that in the stretching and compression zones increases by 89% and 85%, respectively. On the one hand, when the flange length increases, the height h of the flange edge which comes in contact with the roll increases and therefore the edge rises further away from the initial plane of the sheet and its deformation begins earlier (Fig. 12b). On the other hand, the stiffness of the flange decreases by increasing the flange length F. Hence, the deformation begins earlier and intensifies especially in noncontact area with bigger flanges and, consequently, longer deformation lengths are formed in all the regions.

4.5 Effect of sheet thickness *t*

The effect of the sheet thickness on the deformation length in the different regions of the variable cross-section profile and the longitudinal strain during the deformation of the stretching zone can be found by observing Fig. 13. The results indicate that when the thickness increases from 0.5 mm to 1.5 mm, the deformation length shows the decreases of 13% in the narrow and wide sections and of 14% and 24% in the stretching and compression zones, respectively.

According to Fig. 13b, as the sheet thickness increases, the longitudinal strain in the part of the flange edge where is in contact with the roll increases because the flange edge in this area is more subjected to a bending deformation in which the strain increases with a higher thickness. However,

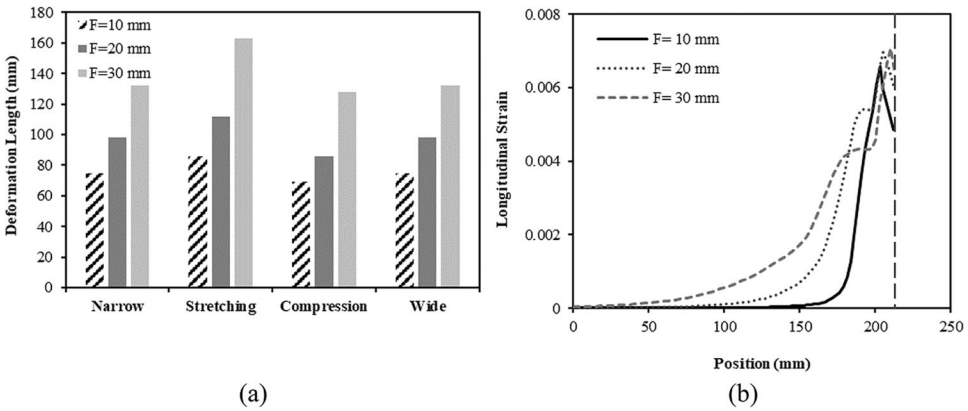

Fig. 12 Effects of flange length F on the deformation length (**a**) and the longitudinal strain along the path at the flange edge when forming the stretching zone (**b**)

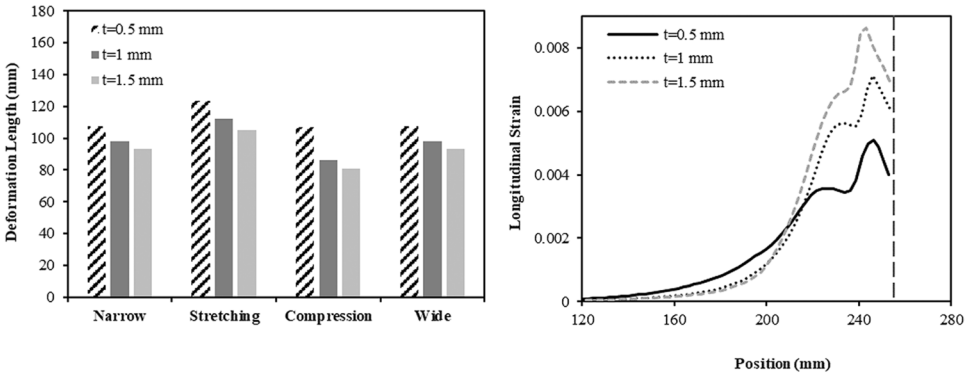

(a) (b)

Fig. 13 Effects of thickness *t* on the deformation length (**a**), and the longitudinal strain along the path at the flange edge when forming the stretching zone (**b**)

a thicker sheet is deformed later and less in the non-contact area due to its greater resistance to a uniaxial tension dominated in this area. As a result of this, the deformation length decreases with the increase of the sheet thickness.

4.6 Effect of yield strength *Y*

The evolution of the deformation length in the different regions of the variable cross-section profile with the yield strength *Y* of the sheet are shown in Fig. 14a. With the increase of yield strength from 150 to 650 MPa, the deformation length increases by 14% in the narrow and wide sections. The increases of the deformation length in the stretching and compression zones are 22% and 30%, respectively, that is higher than that in the constant cross-section regions.

Figure 14b provides the longitudinal strain on the path at the flange edge for the three different yield strengths when the stretching zone is formed. As seen, because of the increase in the resistance to the deformation with a higher yield strength, the longitudinal strain decreases in the contact area, while this resistance causes a larger portion of the flange edge to be loaded in the noncontact area. This is why the deformation length in all the four regions of the profile increases with the increase of the yield strength. However, due to the fact that a more deformation is required to achieve the desired geometries in the stretching and compression zones, a greater increase in the deformation length is obtained in the transition section.

5 Conclusion

In this paper, the deformation length in the flexible roll forming process was numerically and experimentally investigated and its relationship with the deformations applied to the flange edge was determined. Results showed that as the cross-section of a profile changes, the flange edge is subjected to different amounts of the deformations due to varying the flange shape. As a result of this, the different values for the peak longitudinal strain are obtained during the deformation of the variable cross-section channel profile. It was also found that the higher the peak longitudinal strain, the longer the deformation length is formed. For this reason, the maximum and minimum deformation lengths were measured in the stretching and compression zones, respectively, while the deformation lengths were almost equal in the narrow and wide regions. Moreover, results showed that the studied parameters affect the deformation length by changing the edge path or flange resistance, or both. However, the geometric parameters have a greater effect on the deformation length

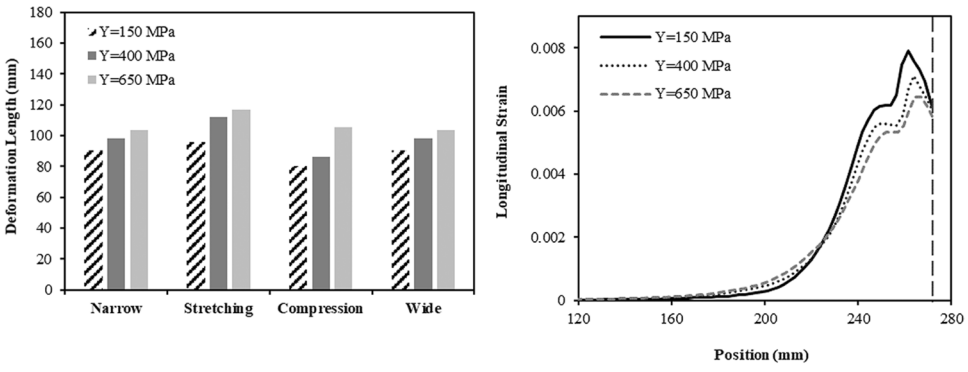

(a) (b)

Fig. 14 Effects of yield strength *Y* on the deformation length (**a**) and the longitudinal strain along the path at the flange edge when forming the stretching zone (**b**)

compared to the material properties. In a future work, the results of this study will be used for developing a relationship for the deformation length in the flexible roll forming process.

Acknowledgements Mohammad Mehdi Kasaei gratefully acknowledges the funding provided by Operation NORTE-06-3559-FSE-000107–Contratação de Recursos Humanos Altamente Qualificados (PME ou CoLAB), supported by Norte 2020 through Fundo Social Europeu. The authors would like to acknowledge the support provided by Tarbiat Modares University.

Funding The present research work was financially supported by Tarbiat Modares University. This study was also funded by Operation NORTE-06–3559-FSE-000107–Contratação de Recursos Humanos Altamente Qualificados (PME ou CoLAB), supported by Norte 2020 through Fundo Social Europeu.

Data availability The authors confirm that the data and material supporting the findings of this study are available within the paper.

Declarations

Competing interests The authors declare no competing interests.

References

1. ShiraniBidabadi B, Moslemi Naeini H, Azizi Tafti R, Barghikar H (2016) Experimental study of bowing defects in pre-notched channel section products in the cold roll forming process. Int J Adv Manuf Technol 87(1):997–1011. https://doi.org/10.1007/s00170-016-8547-y
2. Kasaei MM, Moslemi Naeini H, Abbaszadeh B, Silva MB, Martins PAF. Flexible roll forming. In: Davim JP, editor. Materials dorming and machining: woodhead publishing; 2015. p. 51–71. https://doi.org/10.1016/B978-0-85709-483-4.00003-X
3. Storbeck M, Beiter P, Berner S, Brenneis M, Schmitt W, Groche P, editors. Lightweight products by load optimized profile design. Future Trends in Production Engineering; 2013 2013//; Berlin, Heidelberg: Springer Berlin Heidelberg. https://doi.org/10.1007/s00170-022-09600-7
4. Essa A, Abeyrathna B, Rolfe B, Weiss M (2022) Prototyping of straight section components using incremental shape rolling. Int J Adv Manuf Technol 121(5):3883–3901. https://doi.org/10.1007/s00170-022-09600-7
5. Halmos GT. Roll forming handbook: Crc Press; 2005.
6. Bhattacharyya D, Smith P, Yee C, Collins I (1984) The prediction of deformation length in cold roll-forming. J Mech Working Technol 9(2):181–91. https://doi.org/10.1016/0378-3804(84)90004-4
7. Tafti RA, Naeini HM, Tehrani MS, Rolfe BF, Weiss M (2013) Theoretical extension of elastic-perfectly plastic deformation length in roll forming of a channel section. Int J Mater Prod Technol 47(1–4):33–45
8. Liu C-f, Zhou W-l, Fu X-s, Chen G-q (2015) A new mathematical model for determining the longitudinal strain in cold roll forming process. Int J Adv Manuf Technol 79(5):1055–1061. https://doi.org/10.1007/s00170-015-6845-4
9. Abeyrathna B, Rolfe B, Hodgson P, Weiss M (2016) An extension of the flower pattern diagram for roll forming. Int J Adv Manuf Technol 83(9):1683–1695. https://doi.org/10.1007/s00170-015-7667-0
10. Sun Y, Li Y, Daniel WJ, Meehan PA, Liu Z, Ding S (2017) Longitudinal strain development in chain-die forming AHSS products: analytical modelling, finite element analysis and experimental verification. J Mater Process Technol 243:322–334. https://doi.org/10.1016/j.jmatprotec.2016.12.019
11. Qian Z, Sun Y, Li Y, Wang C, Meehan PA, Daniel WJ et al (2020) Investigation of the design process for the Chain-die forming technology based on the developed multi-stand numerical model. J Mater Process Technol 277:116484. https://doi.org/10.1016/j.jmatprotec.2019.116484
12. Kasaei MM, Naeini HM, Abbaszadeh B, Mohammadi M, Ghodsi M, Kiuchi M et al (2014) Flange wrinkling in flexible roll forming process. Procedia Engineering 81:245–250. https://doi.org/10.1016/j.proeng.2014.09.158
13. Kasaei M, Naeini HM, Liaghat G, Silva C, Silva M, Martins P (2015) Revisiting the wrinkling limits in flexible roll forming. J Strain Anal Eng Design 50(7):528–541. https://doi.org/10.1177/0309324715590956
14. Rezaei R, Moslemi Naeini H, Tafti RA, Kasaei MM, Mohammadi M, Abbaszadeh B (2017) Effect of bend curve on web warping in flexible roll formed profiles. Int J Adv Manuf Technol 93(9):3625–3636. https://doi.org/10.1007/s00170-017-0784-1
15. Woo YY, Han SW, Hwang TW, Park JY, Moon YH (2018) Characterization of the longitudinal bow during flexible roll forming of steel sheets. J Mater Process Technol 252:782–794. https://doi.org/10.1016/j.jmatprotec.2017.10.048
16. DadgarAsl Y, Sheikhi M, PourkamaliAnaraki A, Panahizadeh RV, Hoseinpour GM (2017) Fracture analysis on flexible roll forming process of anisotropic Al6061 using ductile fracture criteria and FLD. Int J Adv Manuf Technol 91(5):1481–1492. https://doi.org/10.1007/s00170-016-9852-1
17. DadgarAsl Y, Woo YY, Kim Y, Moon YH (2020) Non-sorting multi-objective optimization of flexible roll forming using artificial neural networks. Int J Adv Manuf Technol 107(5):2875–2888. https://doi.org/10.1007/s00170-020-05209-w
18. Kasaei MM, Moslemi Naeini H, Abbaszadeh B, Roohi AH, Silva MB, Martins PA (2021) On the prediction of wrinkling in flexible roll forming. Int J Adv Manuf Technol 113(7):2257–2275. https://doi.org/10.1007/s00170-021-06790-4
19. Abeyrathna B, Ghanei S, Rolfe B, Taube R, Weiss M (2022) Optimising part quality in the flexible roll forming of an automotive component. Int J Adv Manuf Technol 118(9):3361–3373. https://doi.org/10.1007/s00170-021-08176-y